OFDM Pilot-Based Radar for Joint Vehicular Communication and Radar Systems

Ceyhun D. Ozkaptan, Eylem Ekici
Dept. of Electrical and Computer Engineering
The Ohio State University
Columbus, OH, USA
ozkaptan.1@osu.edu, ekici.2@osu.edu

Onur Altintas, Chang-Heng Wang
Toyota InfoTechnology Center,
USA, Inc.
Mountain View, CA, USA
onur@us.toyota-itc.com, chwang@us.toyota-itc.com

***Abstract*—With the large-scale deployment of connected and autonomous vehicles, the demand on wireless communication spectrum increases rapidly in vehicular networks. Due to increased demand, the allocated spectrum at the 5.9 GHz band for vehicular communication cannot be used efficiently for larger payloads to improve cooperative sensing, safety, and mobility. To achieve higher data rates, the millimeter-wave (mmWave) automotive radar spectrum at 76-81 GHz band can be exploited for communication. However, instead of employing spectral isolation or interference mitigation schemes between communication and radar, we design a joint system for vehicles to perform both functions using the same waveform. In this paper, we propose radar processing methods that use pilots in the orthogonal frequency-division multiplexing (OFDM) waveform. While the radar receiver exploits pilots for sensing, the communication receiver can leverage pilots to estimate the time-varying channel. The simulation results show that proposed radar processing can be efficiently implemented and meet the automotive radar requirements. We also present joint system design problems to find optimal resource allocation between data and pilot subcarriers based on radar estimation accuracy and effective channel capacity.**

I. Introduction

With the extensive research and industrial initiatives, Intelligent Transportation Systems (ITS) start to evolve into the large-scale deployment of connected vehicles and intelligent infrastructures with roadside units (RSU). For vehicle-to-vehicle (V2V) and vehicle-to-infrastructure (V2I) communication capabilities in ITS, Dedicated Short-Range Communication (DSRC) is designed to improve road safety and traffic management via low-latency exchange of safety messages in the 5.9 GHz spectrum band with 75 MHz bandwidth [1]. As an alternative, Cellular-V2X (C-V2X, also referred to as LTE-V2X) has been designed for vehicle-to-everything (V2X) communication based on Long-Term Evolution (LTE) that provides both cellular and direct communication interfaces [2].

Considering the increase in the number of connected vehicles and roadside units, especially in urban areas, the bandwidth allocated for 5.9 GHz spectrum cannot be used efficiently for non-safety related data or larger payloads along with high priority safety messages and basic sensor/location data. As cooperative sensing and fully autonomous driving technologies gain acceptance, the exchange of a large amount of sensor data is needed for better performance [3]. Higher data rates can be attained by allocating larger bandwidth which is available in the 24 GHz ultra-wideband (UWB) and millimeter-wave (mmWave) spectrums.

Since 24 GHz UWB frequency bands will be phased out by European Telecommunications Standards Institute (ETSI) and the Federal Communications Commission (FCC), 76-77 GHz and 77-81 GHz mmWave spectrum are allocated for the vehicular long-range radar (LRR) and short-range/medium-range radar (SRR/MRR), respectively [4]. The mmWave radar spectrum enables better sensing resolution and accuracy in terms of range, velocity, and angle with higher available bandwidth and smaller wavelength. The decrease in wavelength also allows smaller size antenna arrays for automotive systems.

As higher bandwidth is required by both communication and radar systems to achieve higher data rate and better estimation accuracy, the most direct solution is the spectral isolation of two systems via regulations. In addition, the implementation of interference mitigation and avoidance schemes have been proposed to allow co-existence [5], [6]. As an alternative, designing a joint communication and radar system that can use the same waveform for both sensing and data transmission can eliminate mutual interference. Employing such a joint system will also reduce cost and hardware size while promoting effective utilization of the spectrum.

In this paper, we design a joint system that can perform sensing and communication without mutual interference and performance degradation. Considering high bandwidth requirement and high mobility in the vehicular channel, the communication system must be robust to channel variations and frequency-selectivity due to multi-path propagation [7]. Hence, the orthogonal frequency-division multiplexing (OFDM) waveform is widely employed in mobile communication systems including DSRC due to its spectral efficiency, low-complexity equalization and robustness to frequency-selectivity. We investigate the OFDM signal as a joint waveform to exploit pilot symbols for radar processing and channel estimation while transmitting data in other subcarriers.

Over the past decade, numerous waveform design and processing methods have been proposed for joint communication and radar systems. Linear frequency modulated (LFM) waveform, which is the most commonly used waveform in radar systems, is investigated as an integrated waveform.

978-1-5386-9428-2/18/$31.00 ©2018 IEEE

While some of proposed approaches have leveraged spread-spectrum methods [8], [9] for simultaneous transmission, other studies have employed phase-coding methods [10], [11] to encode data on LFM waveform. However, proposed solutions compromise both communication and radar performance due to interference and the arbitrary encoding of data.

Radar processing methods that exploit communication waveforms have also been proposed in the literature. In [12], IEEE 802.11ad-based radar processing has been investigated to exploit the preamble of single carrier communication frames for vehicular radar systems. Due to dependency on the preamble of single carrier waveform, it lacks the resilience against frequency-selective fading and inter-symbol interference (ISI) which limit the flexibility of the joint system. Furthermore, several OFDM-based radar processing methods are proposed as a joint system in [13] [14] and passive radar system in [15]. In [14], the modulation symbol-based processing has been proposed for monostatic vehicular radar in 24 GHz with 100 MHz bandwidth. The proposed method estimates the range and velocity based on the phase and frequency shifts on modulation symbols with Fourier transforms. Thus, increasing the bandwidth for higher data rate shortens the symbol duration and limits the velocity resolution per symbol. Increasing the number of symbols processed for better resolution increases the memory requirements and computational complexity. Since no pulse compression is used for detection, a higher number of samples is also required to be processed for accurate detection of targets.

In this work, we propose OFDM pilot-based radar processing methods for joint vehicular communication and radar systems that can operate at 76-81 GHz frequency bands. The proposed radar processing can enable vehicles and RSUs to sense their surroundings by leveraging pilot symbols that are employed in many communications standards to carry training symbols. Different from previous approaches, our method combines the matched filtering detection with the 2D Fourier transform to coherently integrate reflected pilot symbols. With coherent integration, the radar estimation can be performed efficiently without sacrificing the processing gain. With the same waveform, the communication receiver can demodulate data while estimating the varying vehicular channel with pilot symbols. Contributions of our work are threefold. First, we propose two pilot-based radar processing methods for (i) *continual pilots* and (ii) *stepped pilots* in OFDM pulses for accurate radar sensing (Section III-A and III-C). Second, we analyze and simulate their performance concerning automotive radar requirements (Section III-B and VI-A). We show that the proposed processing algorithm can comply with the requirements of LRR, MRR, and SRR. Third, we present and solve design problems based on performance metrics of *radar estimation accuracy* and *effective channel capacity* with channel estimation error (Section V and VI-B).

II. System Model

In this section, we describe our system model by formulating the transmitted OFDM signal to carry data and pilot symbols through orthogonal subcarriers. As illustrated in Figure 1, we assume that the transmitter vehicle is also the radar receiver that leverages pilot carriers of the reflected waveform to generate a range-Doppler map of its surroundings. At the same time, the transmitter vehicle also uses the same signal to transmit data to the communication receivers. For simplicity, we assume that radar cross sections (RCS) of targets contain single point scatterers that are nonfluctuating during coherent processing interval (CPI). Given that CPI is not very long, it is safe to assume that the range and velocity of the targets are constant within a CPI as explained in [16, Ch. 8].

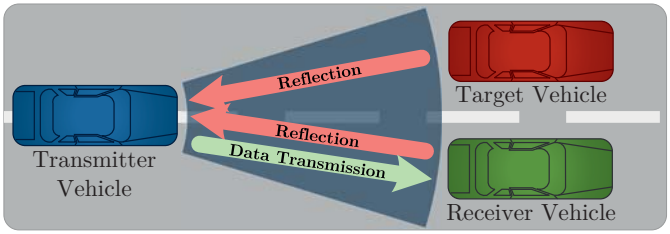

Fig. 1. The operation of the joint communication and radar system on a vehicle (Blue) where it generates the range-Doppler map of the illuminated area with reflections while transmitting data to the receiver vehicle.

A. Transmitted Signal

The transmitted OFDM signal uses N subcarriers consisting of N_p pilot and N_d data subcarriers to transmit complex symbols modulated with phase-shift keying (PSK). The radar pulse is comprised of a coherent burst of M OFDM symbols. In a CPI, L pulses are transmitted and processed coherently to obtain a range-Doppler map. While the communication data is randomly generated, the pilot sequence is chosen according to its auto-correlation function with low peak sidelobe ratio (PSLR). Thus, Barker codes are good candidates for phase-coded pilot sequences with 1:M PSLR [16, Ch. 20]. The proposed baseband OFDM signal can be generated by the inverse discrete Fourier transform (IDFT) and expressed in the continuous-time domain as

$$x(t) = \sum_{l=0}^{L-1} \sum_{m=0}^{M-1} \sum_{n=0}^{N-1} S[n,m,l] g\big(t - mT_{sym} - l\,T_{PRI}\big) \times \exp\big(j2\pi n \Delta f (t - l\,T_{PRI})\big), \quad (1)$$

where $g(t)$ is the pulse shaping function, $\Delta f = 1/T$ is the subcarrier frequency spacing, T is the OFDM symbol duration without cyclic prefix, $T_{sym} = T + T_{cp}$ is the total OFDM symbol duration with cyclic prefix, T_{PRI} is the pulse repetition interval (PRI) as depicted in Figure 2.

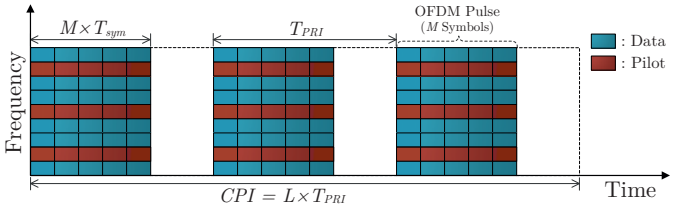

Fig. 2. The structure of the proposed OFDM signal model with continual pilots where $M = 5,\ L = 3,\ N = 9,\ N_p = 3,\ N_d = 6$.

Also, $S[n,m,l]$ denotes the modulated symbols comprised of pilot and data symbols with the indices of the subcarrier, OFDM symbol, and pulse, respectively. The baseband signal is upconverted to the carrier frequency f_c for transmission as

$$x_{rf}(t) = \mathrm{Re}\big\{x(t)\exp(j2\pi f_c t)\big\}. \tag{2}$$

After transmitting M OFDM symbols in MT_{sym} seconds, the transmission is turned of for $T_{off} = T_{PRI} - MT_{sym}$ seconds. The purpose of T_{off} is to estimate Doppler with improved resolution, and allocate time for the preamble.

B. Received Radar Signal

After the signal is reflected from a moving target, it is downconverted to the baseband and the received baseband signal is can be formulated as

$$y(t) = \sigma_{rcs}x(t-\tau)\exp(-j2\pi f_c\tau), \tag{3}$$

where σ_{rcs} is the RCS of the target and $\tau = 2(R-vt)/c$, where R the distance between the target and transmitter, v is the relative radial velocity of the target, and c is the speed of light. By critically sampling the received signal at $t = kT + mT_{sym} + l\,T_{PRI}$, the received signal is discretized as

$$\begin{aligned} y[k,m,l] = \sigma_{rcs}&\sum_{n=0}^{N-1} S[n,m,l]\exp\big(j2\pi n\Delta f k T/N\big) \\ &\times \exp\big(-j2\pi(f_c+n\Delta f)2R/c\big) \\ &\times \exp\big(j2\pi(f_c+n\Delta f)(mT_{sym}+l\,T_{PRI})2v/c\big) \\ &\times \exp\big(j2\pi(f_c+n\Delta f)(kT/N)2v/c\big), \\ k=0,...,N-1,\ m=0,...,M-1,\ l=0,...,L-1.& \end{aligned} \tag{4}$$

As seen in (4), the discrete baseband signal contains four exponents that correspond to the IDFT operation, phase and Doppler shift due to the target's range and velocity. To demodulate OFDM symbols correctly, the orthogonality of the subcarriers must be preserved. However, the fourth exponent of (4) may cause intercarrier interference (ICI) due to Doppler shift. As we choose Δf very large compared to the maximum Doppler shift in the traffic, the effect of the fourth component is negligible. After sampling the received baseband signal, the discrete Fourier transform (DFT) is performed to demodulate the OFDM symbols by canceling the first exponent in (4).

The output of DFT operation can be expressed as

$$\begin{aligned} Y[n,m,l] &= \sum_{k=0}^{N-1} y[k,m,l]\exp\big(-j2\pi nk/N\big) \\ &= \sigma_{rcs}S[n,m,l] \\ &\quad\times \exp\big(-j2\pi(f_c+n\Delta f)2R/c\big) \\ &\quad\times \exp\big(j2\pi(f_c+n\Delta f)(mT_{sym}+l\,T_{PRI})2v/c\big), \\ n=0,...,N-1,\ m=0,...,M-1,\ l=0,...,L-1.& \end{aligned} \tag{5}$$

Equation (5) highlights the effects of range and relative velocity of the target on the transmitted sequence.

III. Pilot-Based Radar Processing

In this section, we present the radar processing methods for pilot sequences in the same and stepped frequency bands of consecutive OFDM pulses. After the reflected signal is demodulated as given in (4) and (5), the pilot sequences in designated subcarriers are matched filtered for pulse compression as expressed in [17, Ch. 11]. With the matched filtering, the OFDM pulses are compressed to detect targets before further compression with 2D IDFT. The ambiguity function (AF) is commonly used to evaluate the output of a matched filter for different delay τ and Doppler υ values [17, Ch. 3]. Narrow mainlobe and low sidelobes along zero-Doppler and zero-delay cuts of the function denote better resolution and detection performance. The AF of pilot-based compression is shown in Figure 3. The zero-Doppler cut shows that the pilot-based compression can achieve an ideal target detection and separation performance. After the detection, the sampled output of the matched filtering can be expressed as

$$\begin{aligned} D[n,i,l] &= \sum_{m=\max(0,i-M+1)}^{\min(i,M-1)} Y\big[\Omega_l[n],m,l\big]\,g_{mf}[i-m] \\ &= \sigma_{rcs}\exp\Big(-j2\pi\big(f_c+\Omega_l[n]\Delta f\big)2R/c\Big) \\ &\quad\times \exp\Big(j2\pi\big(f_c+\Omega_l[n]\Delta f\big)(l\,T_{PRI})2v/c\Big) \\ &\quad\times \Lambda_{mf}[n,i], \\ n=0,...,N_p-1,\ i=0,...,2M-2,\ l=0,...,L-1,& \end{aligned} \tag{6}$$

where

$$\begin{aligned} \Lambda_{mf}[n,i] &= \sum_{m=\max(0,i-M+1)}^{\min(i,M-1)} S_p[m]\,g_{mf}[i-m] \\ &\quad\times \exp\Big(j2\pi\big(f_c+\Omega_l[n]\Delta f\big)(mT_{sym})2v/c\Big) \end{aligned} \tag{7}$$

is the matched filter output, $S_p[m]$ is the phase-coded pilot sequence, and $g_{mf}[m]$ is the matched filter. $\Omega_l[n]$ is used to denote real subcarrier indices of n^{th} pilot sequence on l^{th} OFDM pulse within a CPI. In (6), target's range and velocity introduce linear phase shifts along n (i.e., frequency) and l (i.e., time) axes, respectively. Thus, IDFTs are performed along n and l axes to obtain range-Doppler map and extract target's parameters. But, the position of pilot subcarriers in different pulses (i.e., Ω_l) can affect the radar imaging as covered in Section

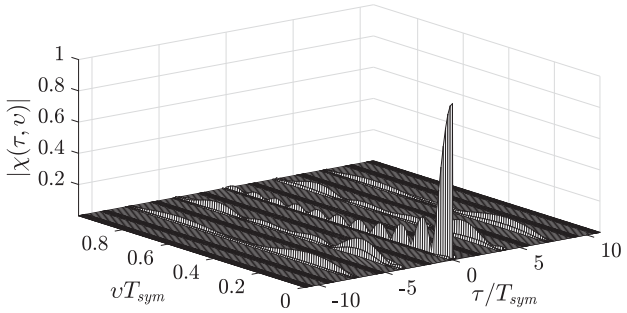

Fig. 3. The ambiguity function of the pilot-based pulse compression with Barker code of length 11 for $N_p = 256, N_d = 768$ with continual pilots.

III-C. In addition, the proposed processing algorithm can be implemented efficiently with 2D IDFT similar to frequency-modulated continuous-wave (FMCW) processing method used in commercial radar sensors [18]. Also note that each pilot sequence in different subcarriers (i.e., n-axis) is affected by both range and Doppler. However, the phase difference caused by the Doppler on different subcarriers is negligible since target's velocities are relatively low and $f_c \gg N\Delta f$.

A. Continual Pilot Processing

In this step, we perform IDFT on OFDM pulses with continual pilot subcarriers. As illustrated in Figure 2, the pilot sequences are equally spaced in frequency and transmitted in the same subcarriers. Therefore, the pilot placement $\Omega_l[n]$ is defined as

$$\Omega_l[n] = n\beta, \quad n = 0,..., N_p-1, \tag{8}$$

assuming $\beta = N/N_p$ is an integer. After the matched filtering, $D[n,i,l]$ is sampled along i-axis at its peaks to acquire $D[n,l]$ with the size of $N_p \times L$. To determine the phase shift due to target's range, IDFTs are computed along n-axis for fixed l values which can be expressed as

$$\begin{aligned} D'[r,l] &= \rho \sum_{n=0}^{N_p-1} D[n,l]\exp\big(j2\pi rn/N_p\big), \\ r &= 0,..., N_p-1, \quad l = 0,..., L-1, \end{aligned} \tag{9}$$

where $\rho = \sigma_{rcs}\Lambda_{mf}$ is the target's RCS and the gain from the matched filtering. Now, $D'[r,l]$ has a single peak along r-axis.

Also, we need to obtain the phase shift due to target's velocity. Hence, IDFT is now performed along l-axis as

$$\begin{aligned} \Psi[r,d] &= \rho \sum_{l=0}^{L-1} D'[r,l]\exp\big(j2\pi dl/L\big), \\ r &= 0,..., N_p-1, \quad d = 0,..., L-1, \end{aligned} \tag{10}$$

where $\Psi[r,d]$ is the complete range-Doppler map with range and Doppler bins denoted by r and d, respectively. As the phase shifts on both axes are highlighted with IDFTs, $\Psi[r,d]$ has a single peak at $(\hat{r},\hat{d})$. To estimate target's range with $\hat{r}$, we first formulate the IDFT of the range component only as

$$\begin{aligned} \mathrm{IDFT}_n\Big(D[n,l]\Big) = \sum_{n=0}^{N_p-1} &\exp\Big(-j2\pi\big(\Omega_l[n]\Delta f\big)2R/c\Big) \\ &\times \exp\big(j2\pi rn/N_p\big), \ r = 0,..., N_p-1, \end{aligned} \tag{11}$$

where $\mathrm{IDFT}_n()$ computes IDFT along n-axis. The peak occurs when the exponents cancel each other. With the index of the peak $\hat{r}$, the range estimate $\hat{R}$ can be derived as

$$\hat{R} = \frac{\hat{r}c}{2N\Delta f}, \quad \hat{r} = 0,..., N_p-1. \tag{12}$$

Similarly, the IDFT of the velocity component only can be expressed as

$$\begin{aligned} \mathrm{IDFT}_l\Big(D[n,l]\Big) = \sum_{l=0}^{L-1} &\exp\big(j2\pi(lf_cT_{PRI})2v/c\big) \\ &\times \exp\big(j2\pi dl/L\big), \quad d = 0,..., L-1. \end{aligned} \tag{13}$$

At the peak index $\hat{d}$, the exponents cancel each other. Assuming the Doppler bins are centered at zero-frequency (i.e., rotated), the velocity estimate $\hat{v}$ can be derived as

$$\hat{v} = \frac{(L/2-\hat{d})c}{2LT_{PRI}f_c}, \quad \hat{d} = 0,..., L-1. \tag{14}$$

B. Radar Performance Metrics

Equation (12) and (14) express how target's range and velocity are estimated based on discrete phase shifts on frequency and time axes, respectively. Therefore, the step size of each equation due to discrete indices determines the resolution performance of the radar processing method. Moreover, the maximum unambiguous range and velocity are determined by the index limits given in (12) and (14). Based on those equations, the range resolution ΔR and velocity resolution Δv are derived as

$$\Delta R = \frac{c}{2B} \ \text{ and } \ \Delta v = \frac{c}{2LT_{PRI}f_c}, \tag{15}$$

respectively. While the range resolution ΔR is determined solely by the total bandwidth $B = N\Delta f$, the velocity resolution Δv is determined solely by $CPI = LT_{PRI}$ considering f_c is fixed. As given in [4], the estimation accuracy for range and velocity can be expressed as

$$\sigma_R = \frac{\Delta R}{2\sqrt{SNR_{rad}}} \ \text{ and } \ \sigma_v = \frac{\Delta v}{2\sqrt{SNR_{rad}}}, \tag{16}$$

in terms of resolutions and signal-to-noise ratio of radar measurements, which is denoted by SNR_{rad}. Since the total transmit power is limited due to regulations, the power allocation between data and pilot subcarriers is investigated for joint system design in Section V. Moreover, the maximum unambiguous range R_{max} and velocity v_{max} are derived as

$$R_{max} = \frac{N_pc}{2B} \ \text{ and } \ v_{max} = \pm\frac{c}{4T_{PRI}f_c}. \tag{17}$$

While estimation accuracy in (16) are the performance metrics of the radar system, the measurement capabilities given in (15) and (17) should be designed to meet the automotive radar requirements summarized in [4], [19]. Based on the requirements of the joint system, trade-offs between radar and communication performance is evaluated in Section IV and V. Nevertheless, we note that R_{max}'s dependence on N_p may limit the performance of the communication system. For instance, increasing N_p for greater R_{max} lowers the communication bandwidth even though it affects the channel estimation performance at the receiver. Thus, we evaluate optimum values of N_p for the joint system design in Section V. Alternatively, pilot sequences can be stepped in frequency bands to increase R_{max}.

C. Stepped Pilot Processing

With continual pilot processing, equally spaced pilots in frequency can achieve high accuracy. However, illuminating the same frequency bands limits R_{max}. Thus, we propose *stepped pilot processing* where pilot sequences are placed in stepped subcarriers to cover all frequency bands available as

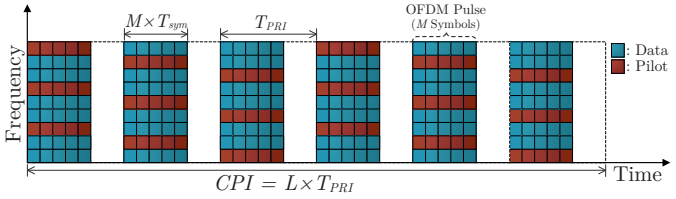

Fig. 4. The structure of OFDM pulses with the stepped pilot sequence where $M = 5,\ L = 6,\ N = 9,\ N_p = 3,\ N_d = 6$.

depicted in Figure 4. While the radar processing is the same for sampling and demodulation in (4) and (5), it differs in the pilot placement $\Omega_l[n]$ and the indexing in data acquisition array $D[n, l]$. So, we redefine the pilot placement $\Omega_l[n]$ as

$$\Omega_l[n] = n\beta + \eta, \quad n = 0,..., N_p-1,\ l = 0,..., L-1, \tag{18}$$

where $\eta = l \bmod \beta$, assuming $\beta = N/N_p$ is an integer and L is a multiple of β. In addition, the indices of $D[n, i, l]$ in (6) are modified as

$$\begin{aligned} D\big[\Omega_l[n], i, \kappa\big] &= \sigma_{rcs}\exp\Big(-j2\pi\big(f_c + \Omega_l[n]\Delta f\big)2R/c\Big) \\ &\quad\times \exp\Big(j2\pi\big(f_c + \Omega_l[n]\Delta f\big)(l\,T_{PRI})2v/c\Big) \\ &\quad\times \Lambda_{mf}[n, i], \\ n = 0,..., N_p-1,\ i &= 0,..., 2M-2,\ l = 0,..., L-1, \end{aligned} \tag{19}$$

where $\kappa = \lfloor l/\beta \rfloor$ is the repetition number and $\Lambda_{mf}[n, i]$ is defined in (7). $D[n, i, l]$ is sampled at its peaks along i-axis to acquire an N-by-(L/β) array. The same processing steps given in Section III-A are followed with N-point and (L/β)-point IDFTs to extract the range and radial velocity, respectively.

However, the stepped pilot subcarriers and target's movement cause distortions that appear as undesired spikes on the estimated range profile. Figure 5 shows the distortions for a target that is located at 62 m and moving with a velocity of 26 m/s. Even if the amplitudes of the spikes are lower than the actual peak, they may be interpreted as targets. Since the pilots are stepped in frequency, each range column of $D[\Omega_l[n], \kappa]$ contains data from different OFDM pulses as formulated in (19). For instance, the matched filtering outputs of the first β pulses in different time indices are placed in the same range bin denoted by its index $\kappa = 0$. But, the second exponent in (19) starts to distort the range estimation due to different l values along the same κ values unlike (6). To uniquely identify the range, we need the target's velocity. Although the range component is affected by the target's movement, the velocity information is not distorted and can be extracted from (19). For instance, the pilot sequence placed in the first subcarrier repeats itself with a period of $\beta\,T_{PRI}$. The repetition in time allows accurate estimation of the velocity. After estimating the velocity, the distortions in the range profile can be removed by eliminating the Doppler distortions along the frequency axis in (19).

While range and velocity resolutions of the stepped pilot processing are the same with continual pilot processing given

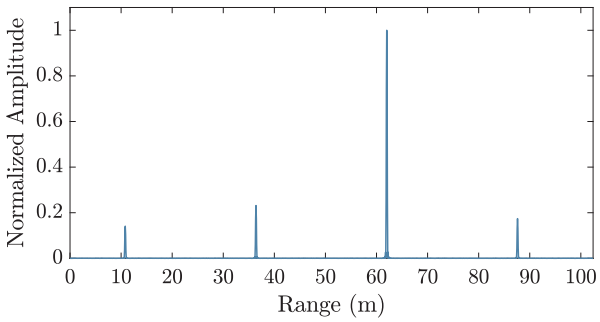

Fig. 5. The distortions on the range profile due to stepped pilots and Doppler

in (15), the maximum unambiguous range and velocity derivations are different. They can be formulated as

$$R_{max} = \frac{\beta N_p c}{2B} \text{ and } v_{max} = \pm\frac{c}{4\beta\,T_{PRI}\,f_c}. \tag{20}$$

Since the pilot sequence is stepped in frequency, the range resolution is multiplied by N to obtain R_{max}. Similarly, the pattern repetition time that is expressed as $\beta\,T_{PRI}$ determines the v_{max} instead of T_{PRI}. Hence, stepped pilot processing trades v_{max} for R_{max} and higher data rate. We assume pilots are stepped through all carriers to maximize R_{max}, but the trade-off can be relaxed by not stepping through all carriers.

IV. Communication Performance

In this section, we evaluate the performance of the communication system based on channel estimation accuracy and channel capacity. The vehicular communication channel is modeled as a frequency-selective channel with finite impulse response (FIR) of length J due to multi-path fading. The discrete FIR can be expressed as

$$\mathbf{h} = [h_1, h_2, \ldots, h_J], \tag{21}$$

where each channel tap is assumed to be independent and identically distributed (i.i.d.) zero-mean complex Gaussian with the variance of σ_h^2. We also consider the communication channel to be time-invariant for at least one OFDM symbol duration T_{sym}, but it can vary between longer periods. Also, the cyclic prefix duration T_{cp} is longer than the maximum delay in the channel to prevent ISI.

Due to variations in the channel, pilot symbols can be used by the receiver to estimate random FIR of the channel. However, the power and subcarrier (i.e., bandwidth) allocations for pilots affect channel estimation accuracy. Imperfect channel estimation at the receiver reduces the effective channel capacity as derived in [20] by taking estimation error into account. Furthermore, allocating more resources to pilots lowers the data transmission rate. Thus, instead of using *ideal* channel capacity formula as the performance metric for communication, we use *effective* channel capacity that integrates the channel estimation error as Gaussian interference as derived in [21].

For the channel estimation, linear minimum mean-square error (LMMSE) estimator $\hat{h}$ is used with the known pilot symbols and channel statistics at the receiver. Based on [20],

the effective channel capacity C_{eff} can be expressed for the joint system as

$$C_{eff} = \gamma N_d \Delta f \log_2 \left(1 + \frac{(P_d/N_d)\sigma_{\hat{H}}^2}{(P_d/N_d)\Phi_e + \sigma_n^2}\right), \tag{22}$$

where P_d is the total power allocated to data subcarriers, σ_n^2 is the variance of the additive white Gaussian noise, $\sigma_{\hat{H}}^2 = J\sigma_h^2 - \Phi_e$ is the variance of the estimator in frequency domain, Φ_e is the variance of the estimation error (i.e., MSE). Also, γ is used to indicate the fraction of time that transmission is active, and it is equal to $(MT_{sym})/T_{PRI} \leq 1$. For $Np \geq J$, the MSE of LMMSE channel estimator is given in [20], [22]

$$\Phi_e = \frac{J\sigma_h^2\sigma_n^2}{\sigma_n^2 + P_p\sigma_h^2}, \tag{23}$$

where P_p is the total power allocated to pilot subcarriers.

V. Joint System Design

In this section, we investigate the performance of the joint communication and radar system as functions of waveform parameters. While the radar system is evaluated by the estimation accuracy for range σ_R and velocity σ_v given in (16), the communication system is evaluated based on effective channel capacity C_{eff} given in (22). Regarding the given performance metrics, the power and subcarrier allocations for pilots and data are the common parameters that can be designed according to performance requirements of the joint system. Moreover, the radar measurement capabilities given in (15) and (17) have to meet radar requirements. Therefore, we present two optimization problems with power allocation parameter $\alpha = P_p/(P_d + P_p)$ and N_p to maximize radar and communication performance with certain constraints.The joint optimization problem that maximizes the communication performance is formulated as

$$\begin{aligned} \max_{N_p,\alpha} \quad & \gamma(N - N_p)\Delta f \log_2 \left(1 + \frac{(J\sigma_h^2 - \Phi_e(\alpha))}{\Phi_e(\alpha) + \frac{(N-Np)}{\xi(1-\alpha)P_t}}\right), \\ \text{s.t.} \quad & \sigma_R \leq \theta_R, \\ & \sigma_v \leq \theta_v, \\ & R_{max} \geq r_{min}, \\ & J \leq N_p \leq N, \\ & 0 < \alpha \leq 1, \end{aligned} \tag{P1}$$

where $P_t = P_d + P_p$ is the total transmit power, ξ is the SNR factor for the received power. Similarly, we formulate another problem that maximizes the radar performance as

$$\begin{aligned} \min_{N_p,\alpha} \quad & \frac{\Delta R}{2\sqrt{SNR_{rad}(\alpha, N_p)}} + \frac{\Delta v}{2\sqrt{SNR_{rad}(\alpha, N_p)}}, \\ \text{s.t.} \quad & C_{eff} \geq c_{min}, \\ & R_{max} \geq r_{min}, \\ & J \leq N_p \leq N, \\ & 0 < \alpha \leq 1, \end{aligned} \tag{P2}$$

TABLE I
Parameters for Different Radar Systems

Parameters	Continual Pilots	Stepped Pilots	
	SRR	MRR	LRR
f_c	79 GHz	79 GHz	76 GHz
B	1.5 GHz	1.5 GHz	0.5 GHz
N	1024	1024	768
N_p	512	256	256
N_d	512	768	512
T	0.68 µs	0.68 µs	1.54 µs
T_{cp}	0.17 µs	0.17 µs	0.38 µs
T_{sym}	0.85 µs	0.85 µs	1.92 µs
T_{off}	2.35 µs	0.64 µs	0.96 µs
T_{PRI}	11.70 µs	3.20 µs	4.80 µs
Bit Rate†	960 Mbps	1440 Mbps	426 Mbps
M	11	3	2
L	280	1024	768
CPI	3.29 ms	3.28 ms	3.68 ms
ΔR	0.10 m	0.10 m	0.30 m
Δv	0.58 m/s	0.58 m/s	0.53 m/s
R_{max}	51 m	102 m	230 m
v_{max}	±81 m/s	±74 m/s	±69 m/s

† Raw bit rate for QPSK modulation without error correction coding.

By solving given optimization problems, we can design an optimal joint waveform for different SNR values due to distance and interference.

VI. Simulations and Numerical Results

In this section, we first present the simulation results for the proposed processing methods to verify the radar performance explained in Section III. For radar simulations, the parameters are chosen according to automotive radar classifications given in [4], [19]. Second, we numerically solved the optimization problems presented in Section V to design joint system parameters for different SNR values.

A. Radar Performance

To assess radar performance, the OFDM waveform is generated based on parameters given in Table I. While data symbols are generated randomly with quadrature phase-shift keying (QPSK) modulation, the pilot sequence is chosen as biphase Barker codes with length M. After OFDM modulation with rectangular pulse shaping, the signal is upconverted to the designated carrier frequency. The phase and Doppler shifts caused by the target's range and velocity are computed with the passband signal. For the baseband processing, the reflected signal is first downconverted and sampled for a CPI duration. The output of the matched filtering with pilot sequences is a 2D array with frequency and time axes. After windowing with Hann function and zero-padding for spectral interpolation, 2D-IDFT of the array is computed to generate the range-Doppler map. Additionally, for the MRR with stepped pilot processing, the velocity is first estimated to eliminate the distortion peaks in the range profile caused by Doppler as shown in Figure 5.

Figure 6 shows the range-Doppler output and the range/Doppler profiles around the peak for SRR configuration with continual pilot processing. For SRR simulation, the target

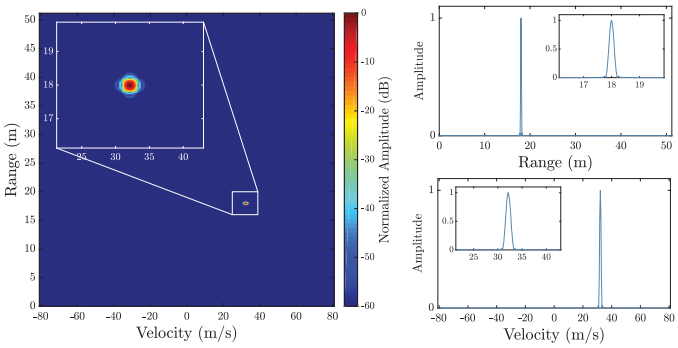

Fig. 6. Continual pilot processing results for SRR parameters

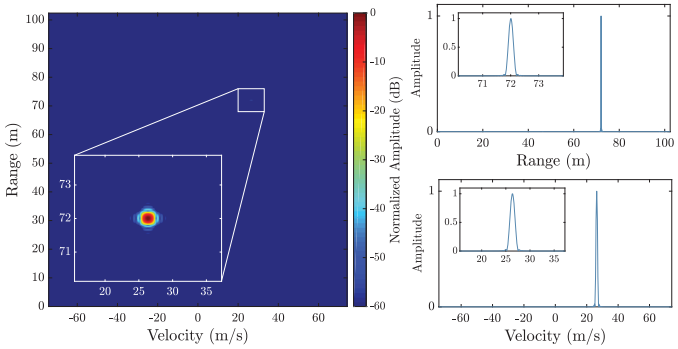

Fig. 7. Stepped pilot processing results for MRR parameters

vehicle is located 18 m away from the transmitter vehicle and moving with relative radial velocity of 32 m/s. For SRR configuration, half of the subcarriers are allocated for pilots to achieve R_{max} of 51 m. However, this lowers the data rate since only the half of the spectrum is used for the data transmission.

For MRR configuration, stepped pilot processing is used to increase the R_{max} without sacrificing bit rate. As shown in Table I, more subcarriers are allocated for the data transmission compared to SRR. The drawback of this method is the increased period of pattern repetition which decreases the v_{max}. However, the decrease in v_{max} can be compensated with shorter pilot sequence which is chosen as $M = 3$. The results of MRR simulation are given in Figure 7 for a target vehicle located 72 m away with a relative radial velocity of 26 m/s. The distortions in Figure 5 are removed by eliminating the Doppler shift on stepped pilots with velocity estimate. The LRR configuration reveals similar behavior as in the case of MRR and has been omitted due to space constraints. In Table I, we show that the proposed processing method can also meet the automotive LRR requirements with lowered bandwidth.

B. Joint Waveform Design

In this section, we present numerical results for the joint design problems described in Section V. For the problems, we use SRR configuration and solve for optimal N_p and α values. We consider that the communication receiver and the target is the same vehicle. The target vehicle has the RCS σ_{rcs} of 20 dBsm and is located at R meters away from the transmitter. We assume that the joint system has the total transmit power P_t of 20 dBm, the noise figure F_n of 15 dB, the transmit G_t and receive $G_{r,rad}$ antenna gain of 15 dB based on [4], [23]. Also, the communication receiver has receive antenna gain $G_{r,com}$ of 30 dB and the same noise figure F_n. The SNR for radar measurements within a CPI is formulated as

$$SNR_{rad} = \frac{(N_p ML)\alpha P_t G_t G_{r,rad} \lambda^2 \sigma_{rcs}}{(4\pi)^3 R^4 k_0 T_0 F_n B}, \tag{24}$$

where k_0 is the Boltzmann's constant, T_0 is the standard temperature. The total number of pilot symbols reflected from the target within a CPI equals to $(N_p ML)$ and determines the processing gain. The SNR factor ξ for the received communication power in (P1) is expressed as

$$\xi = \frac{G_t G_{r,com} \lambda^2}{(4\pi R)^{2.5} k_0 T_0 F_n B N_d / N}, \tag{25}$$

where the path loss exponent is 2.5 and γ is 0.8. For the mmWave communication channel model, we assume the delay spread is 20 ns which generates $J = 30$ channel taps [24].

With given system parameters and SNR equations, the design problems in (P1) and (P2) are numerically solved with MATLAB. We set r_{min} to 50 meters to constraint R_{max} for both problems. First, the effective channel capacity is maximized for different radar accuracy settings: loose ($\theta_R = 1.2 \cdot 10^{-3},\ \theta_v = 7.2 \cdot 10^{-3}$), medium ($\theta_R = 1.0 \cdot 10^{-3},\ \theta_v = 6.0 \cdot 10^{-3}$), tight ($\theta_R = 0.8 \cdot 10^{-3},\ \theta_v = 4.8 \cdot 10^{-3}$).

Figure 8(a) shows that the minimum N_p of 500 is required due to R_{max} constraint. As the distance increases, the received radar power decreases with power of 4. Thus, the power allocated to pilots starts to increase to satisfy the radar constraints as shown in Figure 8(b). However, at low SNRs, N_p also increases along with α for the tight constraints. In Figure 8(c), the optimized C_{eff} is compared with an equal resource allocated system with $N_p = 512$, $\alpha = 0.5$. Figure 8(c) shows the gain of the optimal power allocation from 10 to 50 m where $\alpha = 0.2$ is optimal for C_{eff}. Thus, C_{eff} decreases as α diverges from the optimal value.

For the optimal radar performance, the sum of the range and velocity estimation accuracies is minimized in (P2) with different constraint settings for C_{eff}: loose ($c_{min} = 3.0 \cdot 10^9$), medium ($c_{min} = 3.50 \cdot 10^9$), tight ($c_{min} = 4.0 \cdot 10^9$). At high SNRs, the most of carriers and power are allocated for radar to improve the estimation accuracy as shown in Figure 9. As SNR decreases, the optimal N_p and α values are decreasing in favor of communication performance to satisfy capacity constraint until the minimum N_p is reached. For the tight setting, the minimum N_p is reached after 60 m. Figure 9(c) shows the radar accuracy for the optimized and equal resource allocated OFDM waveform. For the loose and medium constraints, the optimized waveform achieves better estimation accuracy from 10 to 80 m compared to the equal resource allocated waveform. However, the tight setting achieves lower estimation accuracy due to exponential decrease in α after 60 m as the minimum N_p is reached.

VII. Conclusion

In this paper, we investigate the OFDM waveform for joint communication and radar systems to exploit pilot symbols for radar sensing and channel estimation. We propose and analyze two radar processing methods that leverage pilot symbols that are employed in wireless communication systems to estimate

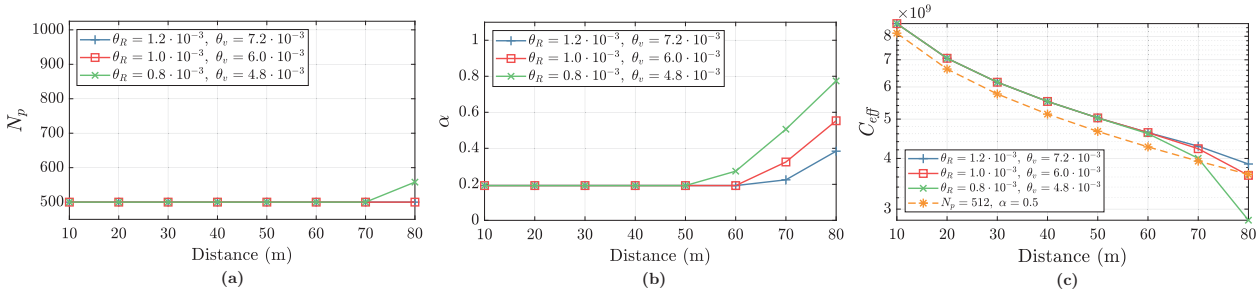

Fig. 8. The numerical results for the design problem that maximizes C_{eff} given in (P1)

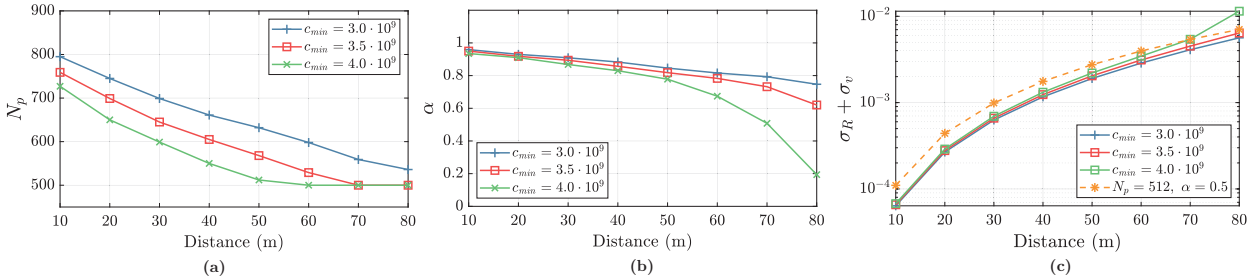

Fig. 9. The numerical results for the design problem that maximizes the radar performance given in (P2)

the time-varying channel. The simulation results demonstrate that the proposed processing methods can achieve high resolution for both range and velocity estimations and comply with the requirements of automotive radar systems operating in 76-81 GHz spectrum band. Moreover, we introduce and solve design problems based on effective channel capacity and radar estimation accuracy to find optimal power and subcarrier allocation for joint systems.

REFERENCES

[1] N. Lu, N. Cheng, N. Zhang, X. Shen, and J. W. Mark, "Connected vehicles: Solutions and challenges," *IEEE Internet of Things Journal*, vol. 1, no. 4, pp. 289–299, Aug 2014.

[2] R. Molina-Masegosa and J. Gozalvez, "Lte-v for sidelink 5g v2x vehicular communications: A new 5g technology for short-range vehicle-to-everything communications," *IEEE Vehicular Technology Magazine*, vol. 12, no. 4, pp. 30–39, Dec 2017.

[3] S. Kim, B. Qin, Z. J. Chong, X. Shen, W. Liu, M. H. Ang, E. Frazzoli, and D. Rus, "Multivehicle cooperative driving using cooperative perception: Design and experimental validation," *IEEE Transactions on Intelligent Transportation Systems*, vol. 16, no. 2, pp. 663–680, April 2015.

[4] J. Hasch, E. Topak, R. Schnabel, T. Zwick, R. Weigel, and C. Waldschmidt, "Millimeter-wave technology for automotive radar sensors in the 77 ghz frequency band," *IEEE Transactions on Microwave Theory and Techniques*, vol. 60, no. 3, pp. 845–860, March 2012.

[5] A. Turlapaty and Y. Jin, "A joint design of transmit waveforms for radar and communications systems in coexistence," in *2014 IEEE Radar Conference*, May 2014, pp. 0315–0319.

[6] K.-W. Huang, M. Bică, U. Mitra, and V. Koivunen, "Radar waveform design in spectrum sharing environment: Coexistence and cognition," in *2015 IEEE Radar Conference (RadarCon)*, May 2015, pp. 1698–1703.

[7] F. Hlawatsch and G. Matz, *Wireless Communications Over Rapidly Time-Varying Channels*, 1st ed. Orlando, FL, USA: Academic Press, Inc., 2011.

[8] Y. Xie, R. Tao, and T. Wang, "Method of waveform design for radar and communication integrated system based on CSS," in *2011 First International Conference on Instrumentation, Measurement, Computer, Communication and Control*, Oct 2011, pp. 737–739.

[9] G. N. Saddik, R. S. Singh, and E. R. Brown, "Ultra-wideband multifunctional communications/radar system," *IEEE Transactions on Microwave Theory and Techniques*, vol. 55, no. 7, pp. 1431–1437, July 2007.

[10] X. Chen, X. Wang, S. Xu, and J. Zhang, "A novel radar waveform compatible with communication," in *2011 International Conference on Computational Problem-Solving (ICCP)*, Oct 2011, pp. 177–181.

[11] M. Nowak, M. Wicks, Z. Zhang, and Z. Wu, "Co-designed radar-communication using linear frequency modulation waveform," *IEEE Aerospace and Electronic Systems Magazine*, vol. 31, no. 10, pp. 28–35, October 2016.

[12] P. Kumari, J. Choi, N. González-Prelcic, and R. W. Heath, "Ieee 802.11ad-based radar: An approach to joint vehicular communication-radar system," *IEEE Transactions on Vehicular Technology*, vol. 67, no. 4, pp. 3012–3027, April 2018.

[13] D. Garmatyuk, J. Schuerger, K. Kauffman, and S. Spalding, "Wideband OFDM system for radar and communications," in *2009 IEEE Radar Conference*, May 2009, pp. 1–6.

[14] C. Sturm and W. Wiesbeck, "Waveform design and signal processing aspects for fusion of wireless communications and radar sensing," *Proceedings of the IEEE*, vol. 99, no. 7, pp. 1236–1259, July 2011.

[15] C. R. Berger, B. Demissie, J. Heckenbach, P. Willett, and S. Zhou, "Signal processing for passive radar using ofdm waveforms," *IEEE Journal of Selected Topics in Signal Processing*, vol. 4, no. 1, pp. 226–238, Feb 2010.

[16] M. Richards, W. Holm, and J. Scheer, *Principles of Modern Radar: Basic Principles*, ser. Electromagnetics and Radar. Institution of Engineering and Technology, 2010.

[17] N. Levanon and E. Mozeson, *Radar Signals*, ser. Wiley - IEEE. Wiley, 2004.

[18] K. Ramasubramanian, "Using a complex-baseband architecture in fmcw radar systems," *Texas Instruments*, 2017.

[19] M. S. Greco, "Automotive radar," in *2012 IEEE Radar Conference, Atlanta, USA*, 2012.

[20] S. Ohno and G. B. Giannakis, "Capacity maximizing mmse-optimal pilots for wireless ofdm over frequency-selective block rayleigh-fading channels," *IEEE Transactions on Information Theory*, vol. 50, no. 9, pp. 2138–2145, Sept 2004.

[21] B. Hassibi and B. M. Hochwald, "How much training is needed in multiple-antenna wireless links?" *IEEE Transactions on Information Theory*, vol. 49, no. 4, pp. 951–963, April 2003.

[22] S. M. Kay, *Fundamentals of Statistical Signal Processing: Estimation Theory*. Upper Saddle River, NJ, USA: Prentice-Hall, Inc., 1993.

[23] J. Jang, J. Oh, C. Kim, and S. Hong, "A 79-ghz adaptive-gain and low-noise uwb radar receiver front-end in 65-nm cmos," *IEEE Transactions on Microwave Theory and Techniques*, vol. 64, no. 3, pp. 859–867, March 2016.

[24] T. S. Rappaport, G. R. MacCartney, M. K. Samimi, and S. Sun, "Wideband millimeter-wave propagation measurements and channel models for future wireless communication system design," *IEEE Transactions on Communications*, vol. 63, no. 9, pp. 3029–3056, Sept 2015.